Available online at www.sciencedirect.com

ScienceDirect

Ceramics International 39 (2013) 9187–9194

CERAMICS INTERNATIONAL

www.elsevier.com/locate/ceramint

Room temperature fatigue of ZrB_2–SiC ceramic composites

M. Lugovy[a,b], N. Orlovskaya[b,*], M. Neubert[c,d], C.G. Aneziris[c], T. Graule[d], J. Kuebler[d]

[a]*Institute for Problems of Materials Science, 3 Krzhizhanivskii Street, 03142 Kyiv, Ukraine*
[b]*University of Central Florida, Orlando, 4000 Central Florida Blvd., Orlando, FL 32816, USA*
[c]*TU Bergakademie Freiberg, D-09596 Freiberg, Germany*
[d]*Empa, Swiss Federal Laboratories for Materials Science and Technology, Laboratory for High Performance Ceramics, Ueberlandstrasse 129, 8600 Duebendorf, Switzerland*

Received 26 April 2013; accepted 5 May 2013
Available online 14 May 2013

Abstract

Room temperature time dependent properties of ZrB_2–30 wt%SiC ceramic composite have been studied. Both static slow crack growth and cyclic fatigue deformation have been investigated. While static slow crack growth has been evaluated only in air, three different environments, water, air, and dry air, have been used to study the cyclic fatigue. It was established that under cyclic fatigue the environment plays an important role and humidity significantly facilitate crack growth in ZrB_2–30wt%SiC. The fractography of selected ZrB_2–30wt%SiC samples was performed and it was established that both defects introduced during machining as well as larger defects introduced during the processing served as fracture origins of ceramic composites.

Keywords: B. Composites; C. Fatigue; D. Borides; D. SiC; Fractography

1. Introduction

Significant number of publications appeared in the last decade dealing mostly with instantaneous mechanical properties with a lot of researchers extensively publishing their study on room and high temperature strength, fracture toughness, elastic modulus, as well as oxidation resistance of ZrB_2 based ceramics, e.g. [1–11]. While studying instantaneous mechanical properties of a composite is a good way for better understanding on how the composite performs under different operational conditions, ultimately it is the composite's time dependent long term behavior, which determines its useful lifetime. A slow subcritical crack growth, a time dependent phenomenon where crack growth occurs at a constant applied stress level below that required for instantaneous failure, is known to be especially dangerous for the long term performance of the brittle ceramics. The cycling loading with applied stresses well below critical stress is another dangerous scenario capable of bringing premature failure to the materials employed. However, only a very limited number of studies on time dependent mechanical behavior of ZrB_2 based composites, such as creep and fatigue, are reported [12–18]. High temperature creep of ZrB_2 and ZrB_2+4 wt%Ni was studied in [12]. Both room and high temperature flexural creep of ZrB_2–SiC composites was studied in [13]. A very elegant technique of electrostatic levitation [14] was employed to perform both experimental and modeling study of creep deformation in ZrB_2–SiC composites [15,16]. The cyclic bending of ZrB_2–14 vol%SiC–30 vol%C composites was studied in [17], where diboride specimens exhibited fatigue at stress levels over 85% of the average flexural strength indicating that the ceramics is rather fatigue resistant. The very preliminary results of high temperature fatigue data at 1700 °C measured by a non-contact technique are reported in [18]. Thus, no significant experiments and no detailed knowledge and understanding of time dependent behavior of Ultra High Temperature Ceramic (UHTC) composites currently exists.

A term fatigue is employed to describe a variety of processes that lead to a degradation of mechanical properties with time. For example, static fatigue has been used to describe stress corrosion cracking in glasses and ceramics in the presence of moisture [19–23], cyclic fatigue has been used

*Corresponding author. Tel.: +1 4078235770; fax: +1 4078230208.
E-mail address: Nina.Orlovskaya@ucf.edu (N. Orlovskaya).

0272-8842/$ - see front matter © 2013 Elsevier Ltd and Techna Group S.r.l. All rights reserved.
http://dx.doi.org/10.1016/j.ceramint.2013.05.020

to study long term behavior of ceramics under cyclic loading [24–30], and the term acoustic fatigue has been introduced to describe the damage accumulation by microcracking that occurs in anisotropic ceramics subject to acoustic waves [31]. A number of failure modes are known to be responsible for failure and limited lifetime of ceramic composites. The most important of them are instantaneous failure, subcritical crack growth under static load, cyclic fatigue, thermal fatigue, indentation fatigue, creep fracture, etc. [32,33]. While instantaneous failure occurs when the applied stress becomes equal to the strength of the material, the delayed failure at moderate temperatures at lower stresses than that of the critical stress can be caused either by subcritical crack growth governed by the actual stress intensity factor K_1 (directly proportional to applied stress σ) or by crack propagation under cyclic load governed both by the stress intensity factor range ΔK_1 (directly proportional to the cyclic stress range $\Delta\sigma$) and the so called R-ratio defined as the quotient of minimum and maximum K_1 value (directly proportional to the ratio of maximum and minimum applied stress in cyclic loading). Therefore, the fatigue damage can be described by a relation between the crack growth rate and the stress intensity factor for initial cracks [34]. Long term fatigue degradation could be a serious obstacle for the successful implementation of ceramic components even at low and moderate level of loading where no instantaneous failure can be expected.

The effect of both stress and environment on the behavior of ceramics is well documented [13,35–40]. Convincing results on the effect of both compressive and tensile stress on corrosion and formation of oxide layer during high temperature creep experiments were produced by Talmy [13]. It was clearly shown that oxidation was greatly promoted by tension, when tensile stress is helping to facilitate oxygen diffusion along the grain boundaries. The environmentally assisted delayed failure in glass and ceramics was also studied [20,23,38]. It was well documented that the presence of water in the environment would facilitate slow crack growth and decrease time to failure both in static and dynamic experiments. The reason for such behavior was that the presence of water molecules would promote faster bond breaking at the crack tip under tensile stress. Therefore, it is important to study the time dependent fatigue behavior and evaluate the effect of the water presence on the delayed static and dynamic failure of ZrB_2–SiC ceramics, since, as to the best of our knowledge no such experiments were performed in the past. Thus, the goal of this paper is to present results of room temperature static and cyclic fatigue testing of ZrB_2–30 wt%SiC UHTC composite, where the effect of the water vapor on the cyclic experiments is clarified.

2. Experimental

The static fatigue experiments were performed in a specially built dead–load testing machine utilizing the procedure described in [41]. The four point bending of the $3 \times 4 \times 48$ mm^3 samples were performed at stresses equal to 80%, 83%,

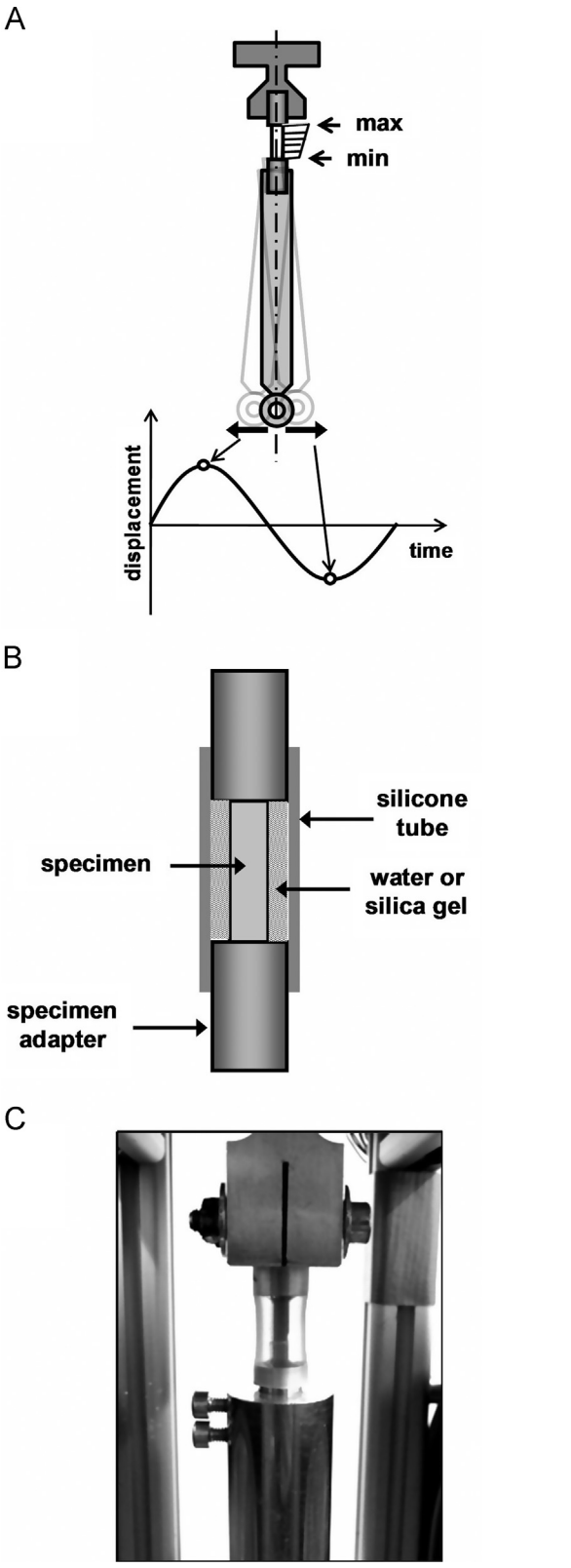

Fig. 1. (A) Schematic drawing of the specimen oscillations in the bending mode during cyclic fatigue experiments. The stress distribution along the length of the sample is also indicated. For the maximum applied stress of 580 (600 or 620) MPa located on the upper end of the sample (max), the corresponding minimum stress of 508 (526 or 544) MPa, respectively, could be found at the end of the lower part of the sample (min); schematic presentation (B) and a photograph of the sample (C) inside the sample holder ready for cyclic fatigue.

and 86% of the Weibull scale parameter $\sigma_0 = 724$ MPa, which was determined using instantaneous mechanical properties of ZrB_2–30 wt%SiC ceramics reported in [6]. Total eleven samples have been tested at each of the three stress levels. The time to failure was recorded for each experiment counting of instantaneous failure as the time equal to zero, and samples, which did not fail after 168 h (7 days) loading at constant stress, were treated as they survived experiment.

The procedure for the cyclic fatigue test is described in [24]. The test allows to perform the cyclic bending of the free end of the rigidly fixed cantilever beam, where a sine waveform stress with constant maximum amplitude σ_{max} is applied. In such loading scheme both surfaces of the sample are alternatively exposed to the equal magnitude tensile and compressive stresses. The tensile stress developed on the sample surface during cycling was calculated using the following equation:

$$\sigma = \frac{Mz}{I}, \quad (1)$$

where M is the applied bending moment, z is the distance between the surface and the neutral axis of the specimen (in this case, $h/2$, where h is the sample height) and I is the moment of inertia (in this case, $wh^3/12$, where w is the sample width). σ_{max} was equal to 80%, 83%, and 86% of the Weibull scale parameter $\sigma_0 = 724$ MPa, which results in 580, 600, and 620 MPa maximum applied stress, with a fixed frequency of 10 Hz ($R = \sigma_{min}/\sigma_{max} = -1$) (Fig. 1A). First 150 loading cycles have not been taken into consideration as the load was slowly build up to the 95% of maximum full load during this period, the failure was classified as instantaneous. One million cycles were chosen as a maximum number of cycles allowed and during the experiment the number of cycles to failure was automatically recorded. It took ~28 h to perform 10^6 cycles.

Three different environments were chose for cyclic fatigue experiments. Aqueous media with 100% relative humidity was the first environment, air with about 30–40% relative humidity was a second chosen environment and a dry air was utilized as the third condition for the experiments. For the first and third set ups the silicone tube was tightly fit over the specimen adapter which was filled either with distilled water or silica gel to remove humidity, respectively. A schematic drawing of the specimen prepared for cyclic testing in water or dry air is shown in Fig. 1B and a photo of the actual sample holder with a sample inside is shown in Fig. 1C. Eleven samples were tested for cyclic fatigue in each media (water, air, and dry air) at each stress amplitude σ_{max}.

3. Results and discussion

3.1. Static fatigue

The results of the static fatigue experiments performed at three pre-selected 580, 600, and 620 MPa constant stress levels are shown in Fig. 2 where the applied stresses are presented against the resulting lifetime to failure in a log–log plot. The samples failed at different time to failure, with some of them

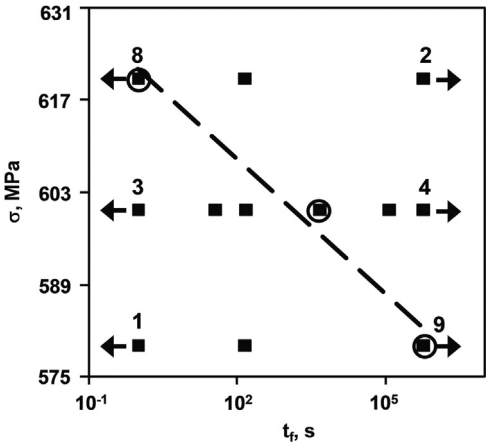

Fig. 2. An applied stress vs. lifetime dependence for static fatigue. The data obtained using a median value technique is presented by a dashed line. Concentric circles indicate median values of eleven data points at each constant applied load and arrows indicate censored data, the value of them are unknown. The numbers above circles indicate number of corresponding censored data points—number of samples either failed instantaneous or did not fail after specified period of experimental time.

failing instantaneous, some of them survived the specified 168 h of testing, and some of the samples failed within specified time period. Such scattering in lifetime correlates to the instantaneous strength scattering as it also depends on the defects' population in the material [34]. The samples which failed instantaneous and did not fail after 168 h were considered as censored data. The numbers of such samples failed outside of the specified time window at a given constant stress are shown in Fig. 2.

To describe results of the static fatigue experiments and, in particular, to determine slow crack growth parameter, the following equation is typically used [34,42]

$$t_f = B\sigma_c^{n-2}\sigma^{-n}, \quad (2)$$

where t_f is the time to failure, B is the material parameter, σ is the applied stress, σ_c is the so called inert strength or the strength without the influence of the slow crack growth, and n is a slow crack growth exponent. In its logarithmic form Eq. (2) reads as

$$\log\ t_f = -n \log\ \sigma + \log\,(B\sigma_c^{n-2}). \quad (3)$$

From Eq. (3) the parameter n can be obtained by linear regression of $\log(t_f)$ versus $\log(\sigma)$. It is known that the value of n at room temperature is usually between ten to several hundred [34]. To ensure a high resistance to subcritical crack growth, the exponent n in Eq. (2) should be as high as possible. The lower it is, the more susceptible a material is to subcritical (slow) crack growth at the prevalent environmental conditions. By using Eq. (3) the value for n, where $-1/n$ is the slope of the straight line joining the median values for time to failure at each static stress level in Fig. 2, was calculated to be 204. Such high value of n exponent in Eq. (3) would be a very good result indicating that ZrB_2–30 wt%SiC ceramic composite is rather resistant to slow crack growth, however not sufficient number of valid data points used for the calculation

of both median values of the lifetimes and n exponent, consequently, provide a high uncertainty in the obtained results.

3.2. Cyclic fatigue

The results of the cyclic fatigue are presented in Fig. 3, where, similar to the static fatigue, the applied stress range is log–log plotted against resulting lifetime/number of cycles to failure. The stress amplitude ranges $\Delta\sigma = 2\sigma_{max}$ were 1160, 1200, and 1240 MPa for testing in water and air, and 1240 MPa for testing in dry air. As one can see from Fig. 3, a large scattering of the lifetime results was obtained at all stress amplitudes of cycling in different environments, similar to the testing performed for the static slow crack growth, as both processing related and machining related defects contributed to the fatigue failure of ZrB_2–30 wt%SiC. In the case of cyclic fatigue, the same as for static fatigue, a number of censored data were collected, with their amount shown in Fig. 3. The presence of censored data affects strongly the location of lifetime median values and as a result affecting the precision in estimation of the fatigue parameters by introducing uncertainties into the calculations.

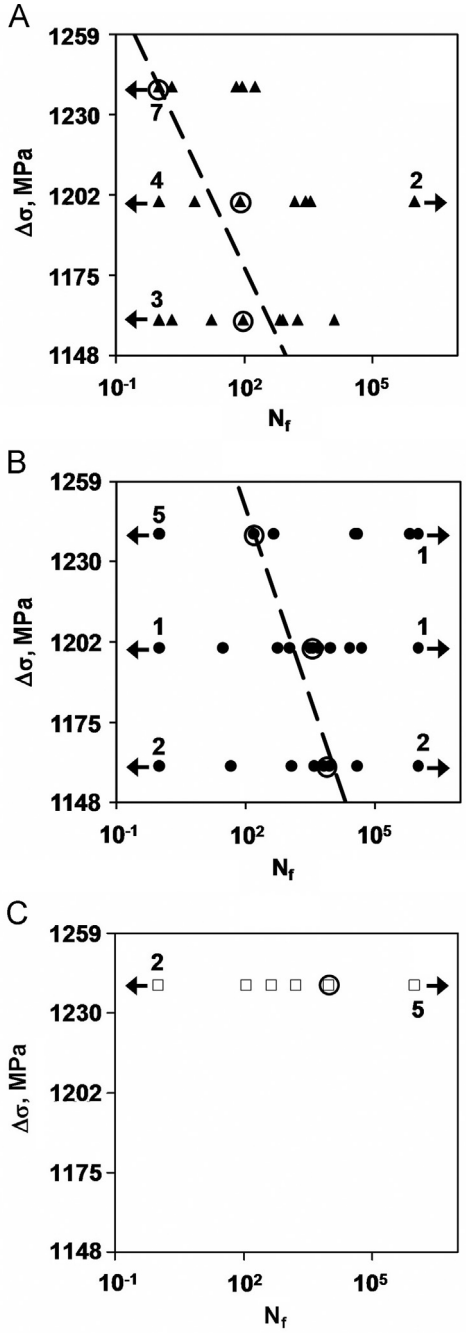

Fig. 3. Stress range vs. cycles to failure for cyclic fatigue in water (A), air (B) and dried air (C). The data obtained using a median value technique is presented by a dashed line. Concentric circles indicate median values of eleven data points at each constant applied load and arrows indicate censored data. The numbers above circles indicate the number of corresponding censored data points—number of samples either failed instantaneous or did not fail after specified number of cycles.

To describe results of the cyclic fatigue experiments in the quantitative way and to determine the cyclic fatigue crack growth parameters, the following equation, a very similar one to the Eq. (2) used in static fatigue experiments, is used [34]

$$N_f = B_c \sigma_c^{n_c-2} \Delta\sigma^{-n_c} \tag{4}$$

where N_f is the cycles to failure, B_c is the material parameter for cyclic fatigue, $\Delta\sigma$ is the stress range, and n_c is the cyclic fatigue crack growth exponent. Similarly, to the static slow crack growth experiments, the conversion of Eq. (4) to the logarithmic form yields the following equation:

$$\log\ N_f = -n_c \log\ \Delta\sigma + \log\left(B_c \sigma_c^{n_c-2}\right) \tag{5}$$

which is used for the calculation of n_c parameter of the cyclic fatigue data. The n_c parameter, calculated in a similar way as n exponent for static fatigue, yields 88 for experiments performed in water and 66 for experiments performed in air. As the experiments in dry air conditions were performed only at one stress range of 1240 MPa, it is simply not enough data to calculate n_c crack growth parameter for the dry air experiments using the proposed method.

The n_c crack growth parameter should be the same for the material tested in media with only different humidity [20,38]. The calculated n_c values, nevertheless, differ significantly in our calculations, as n_c=88 for tests performed in water and n_c=66 for testing in air. Such discrepancy could be explained by a significant number of censored data points contributing to large uncertainties in the n_c exponent calculation. Thus, the existence of seven samples which failed instantaneous for testing at $\Delta\sigma$=1240 MPa stress range in water might well be a reason for increased value of n_c exponent in comparison with the results of testing in air. Also some of the instantaneously failed samples could fail not from surface defects, but from large defects located in the bulk of the ceramic bar, and in such a case that data point should be completely excluded from the consideration, however, while the fractography was performed on selected samples, the fractography of all samples was not done due to time constrains for the experiments. Thus, since the real N_f values are unknown, this brings a rather large uncertainty in the calculated numbers.

Another crack growth parameter

$$A_c = \frac{2K_{1c}^2}{B_c(n_c-2)Y^2} \tag{6}$$

used to estimate the resistance of the material to the crack propagation during the crack growth per cycle as defined by

$$\frac{da}{dN} = A_c\left(\frac{\Delta K_1}{K_{1c}}\right)^{n_c} \tag{7}$$

is important to be determined in addition to the n_c exponent. $\Delta K_1 = \Delta\sigma Y a^{1/2}$ is the range of stress intensity factor, Y=1.29 for a semicircular crack at the surface, a is the crack length, K_{1c} is the fracture toughness (K_{Ic}=3.8 MPa × $m^{1/2}$ [6]). The material parameter B_c was determined as

$$B = \frac{10^{n_c D}}{\sigma_c^{n_c-2}}, \tag{8}$$

where D is the log $(B_c^{1/n_c}\sigma_c^{(n_c-2)/n_c})$ determined as y-coordinate of the point of the straight line joining the median values for cycles to failure at each stress range in Fig. 3 when its x-coordinate is zero, $\sigma_c = \sigma_0(\ln 2)^{1/m}$ is the median value of instantaneous strength, m is the Weibull exponent (6.7 for our material [6]). For our experiments the crack growth parameter A_c was calculated to be equal to 1.05×10^{-17} μm/cycle for testing in water and 2.37×10^{-19} μm/cycle for testing in air.

It is known that the humidity is a strong contributor to enhanced crack growth in brittle solids [20,38], where the increase in humidity brings a significant acceleration of crack growth rate and decrease of the fatigue lifetime. The coefficient A_c=1.05×10^{-17} μm/cycle for the samples tested in water is two orders of magnitude higher than A_c=2.37×10^{-19} μm/cycle for the samples tested in air, indicating much faster crack growth in ZrB_2–30 wt%SiC composite during cyclic fatigue in water in comparison with testing in air. Therefore, the cyclic loading where the samples were tested in water (100% of humidity) shows the fastest crack growth and shortest lifetime in comparison with the tests performed under 30–40% of humidity (standard lab environment). It is expected that, when the moisture is removed by silica gel, which is a strong moisture absorber e.g. used in desiccators for samples storage under dry conditions, the slowest crack growth should be observed for the experiments with dry air conditions.

3.3. Fractography

The typical fracture surface of a sample tested under static slow crack growth is shown in Fig. 4. The sample failed after being held for 37 s at 600 MPa constant applied stress. The optical micrograph (Fig. 4A) shows two parts of the broken bar, where the region containing fracture origin of the sample could be clearly identified. The SEM micrograph of the fracture origin is shown in Fig. 4B. What can be seen from the micrographs is that the defect, where the failure initiated, is located at the surface of the bar. Such surface defects, which further serve as fracture origin during the failure of the material, are most likely introduced during machining of the samples. If we calculate the critical defect size of the material with a known fracture

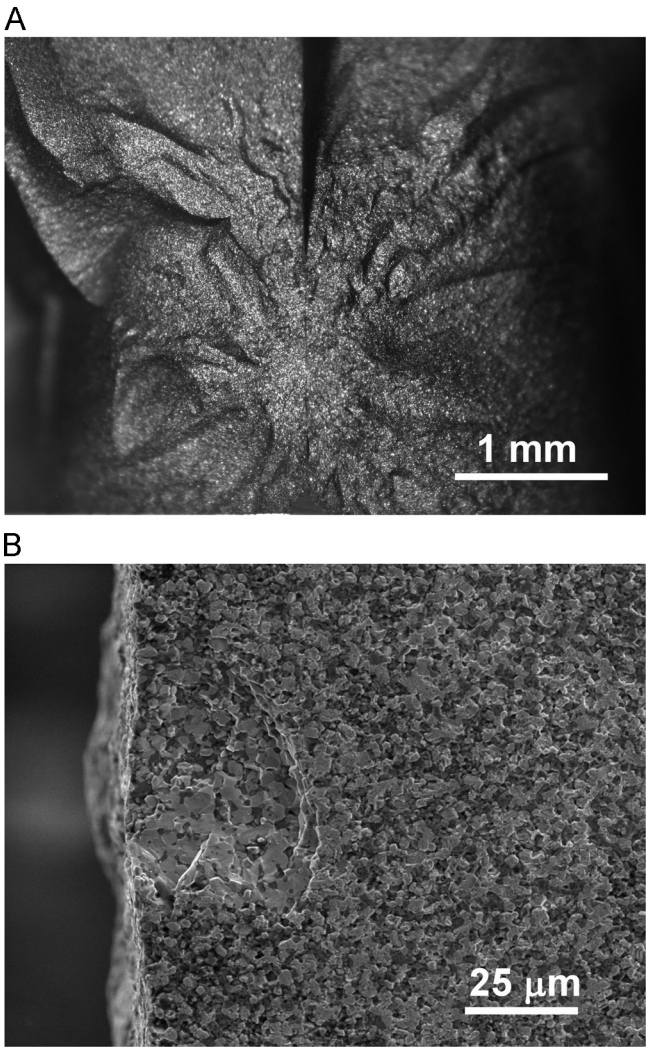

Fig. 4. Fractography of the ZrB_2–30 wt%SiC ceramics composite tested under static slow crack growth conditions. The sample failed after 37 s of static 600 MPa applied stress. (A) An optical micrograph of both fracture surfaces; (B) SEM micrograph of the edge defect introduced by machining which served as a fracture origin of the sample under study.

toughness and critical stress (σ = 600 MPa) values we can compare it with the measured size of the critical defect shown in Fig. 4B. By using the equation $a_c = (K_{1c}/Y\sigma)^2$, with Y = 1.29 for the surface crack, the calculated defect size can be estimated to be equal to 24 μm, which is quite close to the defect dimensions shown in Fig. 4B. The presence of such defects introduced during machining of ceramics is unavoidable. However, if machining of ceramics could be performed using finer diamond wheels or using lower pressure during machining, or, the best, the final surface finish could be made as a mirror like polished surface, the ZrB_2–30 wt%SiC ceramic should exhibit much better long time mechanical behavior.

The defects introduced during machining has also served as fracture origins in ZrB_2–30 wt%SiC ceramics tested in cyclic fatigue, however a few samples failed from larger defects formed during the processing of material. Some of those large defects brought the samples to the failure at the very beginning of the cyclic loading and their failure has been classified as

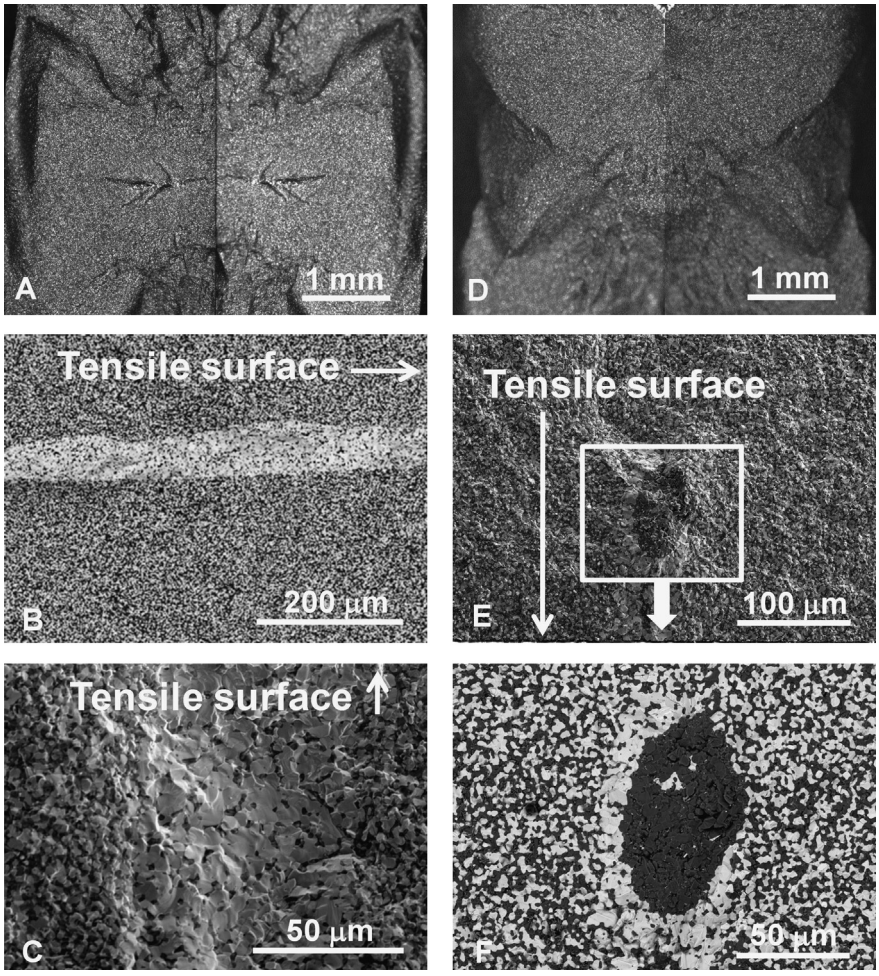

Fig. 5. Fractography of two ZrB_2–30 wt%SiC samples tested during cyclic fatigue. (A–C) A fracture surface of the sample failed due to presence of a large ZrB_2 agglomerate. (A) An optical micrograph of fracture surfaces of the two broken parts, (B) SEM backscattered image of the large ZrB_2 defect, (C) secondary electron image of the defect consisting of porous agglomerate of large ZrB_2 grains. (D–F) A fracture surface of the sample failed due to a presence of a large SiC agglomerate. (D) An optical micrograph of fracture surfaces of the two broken parts, (E) SEM image of a large ZrB_2 defect and (C) backscaterred image of the defect consisting of agglomerate of SiC grains surrounded by ZrB_2 grains.

instantaneous. Using SEM with EDS analysis, it was established that such defects consisted of either ZrB_2- or SiC-based agglomerates appearing during processing of the material due to non-homogeneous mixturing of two components. An example of extremely large fracture origin consisting of ZrB_2 based agglomerate is shown in Fig. 5A–C. The optical micrograph of the defect gives an image of both parts of fractured sample (Fig. 5A). The fracture surface of this sample is relatively flat in comparison with other samples fractured in the experiments and, in addition, the sample failed only into two separate parts after fracture, while most of other samples, which survived certain number of cycling loading, failed into multiple small fragments. The size of this defect is enormous—its length is equal to ~500 μm. The SEM backscattered image of the ZrB_2 defect is presented in Fig. 5B and a secondary electron image of the defect consisting of the large ZrB_2 grains presented in Fig. 5C.

Another type of a defect consisting of large SiC agglomerate is shown in Fig. 5D–F. The sample with SiC defect serving as a fracture origin was loaded at 600 MPa maximum stress and failed after 65 cycles. The optical micrograph of the two parts of the fracture surfaces of the sample is shown in Fig. 5D and SEM images of the critical defect are shown in Fig. 5E and F. As one can see from Fig. 5E the major part of the defect is located in the bulk of the sample, however the defect still propagates toward the surface. The backscattering image shows that the central part of the defect is SiC phase surrounded by agglomeration of ZrB_2 grains (Fig. 5F). By using the equation $a_c=(K_{1c}/Y\sigma)^2$, with $Y=1.47$ for the bulk crack [43], the calculated defect size can be estimated to be equal to 36 μm, which is rather close to the defect dimensions shown in Fig. 5F. The appearance of such defect can be explained by not thorough mixing of the initial powders during the batch preparation, thus there are further opportunities to improve the manufacturing process by better mixing and homogenizing the SiC and ZrB_2 powders.

4. Conclusions

Time dependent room temperature mechanical properties of ZrB_2–30 wt%SiC ceramic composites were studied. Both static

slow crack growth and cyclic fatigue experiments were performed. The static slow crack growth experiments were performed in air, but cyclic fatigue was studied under three different conditions—in water, air and dry air environment. The crack growth parameters were determined and it was estimated that the n exponent, which determines the ability of the material to resist crack propagation under constant or cyclic applied stress, is higher for the static slow crack growth experiments than for the cyclic fatigue tests. However, because of poor statistics, the n parameter, calculated by the median technique, was higher for cyclic tests performed in water, than for cyclic tests performed in air. The second crack growth parameter A, showing the crack growth per single cycle, was by two order of magnitude higher for testing in water in comparison with tests in air, thus indicating much faster degradation rate of ZrB_2–30 wt%SiC when the humidity is 100%. The fractography of the ZrB_2–30 wt%SiC ceramic composites indicated that the majority of the critical defects bringing failure originated from the surface machining, however some huge defects, responsible for material's failure, were introduced also during the processing. Thus, improvement in the machining and processing would bring the improvement in the lifetime of the ceramic composite.

Acknowledgment

This work was supported by the National Science Foundation, Division of Materials Research, project # 0748364 in Ceramics program. Dr. Lugovy's work at Empa was supported by the Swiss National Science Foundation via the International Short Visit fellowship (Decision IZK0Z2_134265) and Mr. M. Neubert was supported by Empa, Lab for High Performance Ceramics internal grant for student research.

References

[1] A.L. Chamberlain, W.G. Fahrenholtz, G.E. Hilmas, D.T. Ellerby, High-strength zirconium diboride–based ceramics, Journal of the American Ceramic Society 87 (2004) 1170–1172.
[2] S. Zhu, W.G. Fahrenholtz, G.E. Hilmas, Influence of silicon carbide particle size on the microstructure and mechanical properties of zirconium diboride—silicon carbide ceramics, Journal of the European Ceramic Society 27 (2007) 2077–2083.
[3] A. Rezzaie, W.G. Fahrenholtz, G.E. Hilmas, Effect of hot pressing time and temperature on the microstructure and mechanical properties of ZrB_2–SiC, Journal of Materials Science 42 (2007) 2735–2744.
[4] F. Monteverde, S. Guicciardi, A. Bellosi, Advances in microstructure and mechanical properties of zirconium diboride–based ceramics, Materials Science and Engineering: A A346 (2003) 310–312.
[5] S.Q. Guo, J.-M. Yang, H. Tanaka, Y. Kagawa, Effect of thermal exposure on strength of ZrB_2-based composites with nano-sized SiC particles, Composites Science and Technology 68 (2008) 3033–3040.
[6] N. Orlovskaya, R. Stadelmann, M. Lugovy, V. Subbotin, G. Subhash, M. Neubert, C.G. Aneziris, T. Graule, J. Kuebler, Mechanical properties of ZrB_2–SiC ceramic composites: room temperature instantaneous behavior, Advances in Applied Ceramics 112 (2013) 9–16.
[7] J.K. Sonber, A.K. Suri, Synthesis and consolidation of zirconium diboride: review, Advances in Applied Ceramics 110 (6) (2011) 321–334.
[8] D.D. Jayaseelan, Y. Wang, G.E. Hilmas, W. Fahrenholtz, P. Brown, W.E. Lee, TEM investigation of hot pressed-10 vol%SiC–ZrB_2 composite, Advances in Applied Ceramics 110 (1) (2011) 1–7.
[9] A.K. Khanra, L.C. Pathak, M.M. Godkhindi, Carbothermal synthesis of zirconium diboride (ZrB_2) whiskers, Advances in Applied Ceramics 106 (3) (2007) 155–160.
[10] A.K. Khanra, M.M. Godkhindi, Effect of Ni additives on pressureless sintering of SHS ZrB_2, Advances in Applied Ceramics 104 (6) (2005) 273–276.
[11] A.K. Khanra, L.C. Pathak, S.K. Mishra, M.M. Godkhindi, Sintering of ultrafine zirconium diboride powder prepared by modified SHS technique, Advances in Applied Ceramics 104 (6) (2005) 282–284.
[12] J.J. Melendez-Matrinez, A. Dominguez-Rodriguez, F. Monteverde, C. Melandri, G. de Portu, Characterisation and high temperature mechanical properties of zirconium boride-based materials, Journal of the European Ceramic Society 22 (2002) 2543–2549.
[13] I. Talmy, J.A. Zaykoski, C.A. Martin, Flexural creep deformation of ZrB_2/SiC ceramics in oxidizing atmosphere, Journal of the American Ceramic Society 91 (5) (2008) 1441–1447.
[14] J.R. Rogers, R.W. Hyers, Electrostatic levitation: an emerging materials characterization technique, in: Presented at the TMS Annual Meeting, 2008.
[15] J. Lee, R.C. Bradshaw, R.W. Hyers, J.R. Rogers, T.J. Rathz, J.J. Wall, H. Choo, P.K. Liaw, Non-contact measurement of creep resistance of ultra-high temperature materials, Materials Science and Engineering: A 463 (1–2) (2007) 185–196.
[16] X. Ye, R.W. Hyers, Computational methods for the analysis of non-contact creep deformation in ZrB_2-SiC composites, Journal of the European Ceramic Society 30 (2010) 2191–2196.
[17] E.L. Strauss, T.F. Kieffer, Strength of zirconium diboride ceramics after cyclic loading or heating, Journal of the American Ceramic Society 58 (1975) 399–401.
[18] S. Gangireddy, J.W. Halloran, Z.N. Wing, Non-contact mechanical property measurements at ultrahigh temperatures, Journal of the European Ceramic Society 30 (2010) 2183–2189.
[19] S.M Wiederhorn, Influence of water vapor on crack propagation in soda–lime glass, Journal of the American Ceramic Society 50 (8) (1967) 407–414.
[20] S.W. Freiman, S.M. Wiederhorn, J.J. Mecholsky Jr., Environmentally enhanced fracture of glass: a historical perspective, Journal of the American Ceramic Society 92 (7) (2009) 1371–1382.
[21] T. Fett, D. Munz, Evaluation of subcritical crack extension under constant loading, Journal of the European Ceramic Society 6 (1990) 67–72.
[22] T. Fett, D. Munz, Determination of v–K_I curves by a modified evaluation of lifetime measurements in static bending tests, Journal of the American Ceramic Society 68 (1985) C213–C215.
[23] C.K.L Daives, F. Guiu, M. Li, M.J. Reece, R. Torrecillas, Subcritical crack propagation under cyclic and static loading in mullite and mullite-zirconia, Journal of the European Ceramic Society 18 (1998) 221–227.
[24] T. Fett, G. Martin, D. Munz, G. Thun, Determination of da/dNâˆ’Î”K1 curves for small cracks in alumina in alternating bending tests, Journal of Materials Science 26 (1991) 3320–3328.
[25] A.G. Evans, E.R. Fuller, Crack propagation in ceramic materials under cyclic loading conditions, Metallurgical Transactions 5 (1974) 27–33.
[26] S. Horibe, R. Hirahara, Cyclic fatigue of ceramic materials: influence of crack path and fatigue mechanisms, Acta Metallurgica et Materialia 39 (1991) 1309–1317.
[27] R. Schmitt, T. Fett, D. Munz, Cyclic fatigue of zirconia, Fatigue and Fracture of Engineering Materials and Structures 19 (1996) 1411–1420.
[28] A. Bushby, F. Guiu, J. Knowles, M.J. Reece, Cyclic fatigue of silicon nitride at 1000 Â°C, Key Engineering Materials 89–91 (1993) 673–678.
[29] J. Bermudo, M.I. Osendi, M. Li, M.J. Reece, Cyclic fatigue behavior of silicon nitride materials, Journal of the European Ceramic Society 17 (1997) 1855–1860.
[30] F. Guiu, M.J. Reece, D.A.J. Vaughan, Cyclic fatigue of ceramics, Journal of Material Science 26 (1991) 3275–3286.
[31] A.G. Evans, Fatigue in ceramics, International Journal of Fracture 16 (1980) 485–498.
[32] T. Fett, D. Munz, Evaluation of subcritical crack extension under constant loading, Journal of the European Ceramic Society 6 (1990) 67–72.

[33] M. Reece, F. Guiu, Indentation fatigue of high-purity alumina in fluid environments, Journal of the American Ceramic Society 74 (1991) 148–154.
[34] D. Munz, T. Fett, Ceramics: Mechanical Properties, Failure Behavior, Materials Selection, Springer, Berlin, Heidelberg, Germany, 2001.
[35] J. Kilner, Feeling the strain, Nature Materials 7 (2008) 838–839.
[36] J. Garcia Barriocanal, A. Rivera-Calzada, M. Varela, Z. Sefrioui, E. Iborra, C. Leon, S.J. Pennycook, J. Santamaria, Colossal ionic conductivity at interfaces of epitaxial ZrO_2:Y_2O_3/$SrTiO_3$ heterostructures, Science 321 (2008) 676–680.
[37] W. Araki, M. Kuribara, Y. Arai, Strain effect on oxygen migration in yttria-stabilized zirconia, ECS Transactions 35 (1) (2011) 1117–1124.
[38] S.M. Wiederhorn, Moisture assisted crack growth in ceramics, International Journal of Fracture Mechanics 4 (2) (1968) 171–177.
[39] F. Guiu, M. Li, M.J. Reece, Role of crack-bridging ligaments in the cyclic fatigue behavior of alumina, Journal of the American Ceramic Society 75 (1992) 2976–2984.
[40] M.J. Reece, F. Guiu, M.F.R. Sammur, Cyclic fatigue crack propagation in alumina under direct tension–compression loading, Journal of the American Ceramic Society 72 (1989) 348–352.
[41] European Standard Final Draft, PREN 843-3, Advanced Technical Ceramics—Monolithic Ceramics, Mechanical properties at room temperature, Part 3, Determination of subcritical crack growth parameters from constant stressing rate flexural strength tests, November 2004.
[42] S. Pathak, D. Steinmetz, J. Kuebler, E.A. Payzant, N. Orlovskaya, Mechanical behavior of $La_{0.8}Sr_{0.2}Ga_{0.8}Mg_{0.2}O_3$ perovskites, Ceramics International 35 (2009) 1235–1241.
[43] C.R. Newman, I.S. Raju, An empirical stress intensity factor equation for the surface crack, Engineering Fracture Mechanics 15 (1–2) (1981) 185–192.